1132–1143 *Nucleic Acids Research, 2001, Vol. 29, No. 5*

A nicked duplex decamer DNA with a PEG_6 tether

L. Kozerski[1,2,*], A. P. Mazurek[1], R. Kawecki[2], W. Bocian[1], P. Krajewski[2], E. Bednarek[1], J. Sitkowski[1,2], M. P. Williamson[3], A. J. G. Moir[3] and P. E. Hansen[4]

[1]Drug Institute, 00-725 Warszawa, Chetmska 30/34, Poland, [2]Institute of Organic Chemistry, Polish Academy of Sciences, 01-224 Warszawa, Kasprzaka 44, Poland, [3]Department of Molecular Biology and Biotechnology, University of Sheffield, Sheffield S10 2TN, UK and [4]Department of Life Sciences and Chemistry, Roskilde University, DK-4000 Roskilde, Denmark

Received October 31, 2000; Revised and Accepted January 12, 2001 PDB no. 1G1N

ABSTRACT

A dumbbell double-stranded DNA decamer tethered with a hexaethylene glycol linker moiety (DDSDPEG), with a nick in the centre of one strand, has been synthesised. The standard NMR methods, E.COSY, TOCSY, NOESY and HMQC, were used to measure ^1H, ^{31}P and T_1 spectral parameters. Molecular modelling using rMD-simulated annealing was used to compute the structure. Scalar couplings and dipolar contacts show that the molecule adopts a right-handed B-DNA helix in 38 mM phosphate buffer at pH 7. Its high melting temperature confirms the good base stacking and stability of the duplex. This is partly attributed to the presence of the PEG_6 linker at both ends of the duplex that restricts the dynamics of the stem pentamers and thus stabilises the oligonucleotide. The inspection of the global parameters shows that the linker does not distort the B-DNA geometry. The computed structure suggests that the presence of the nick is not disturbing the overall tertiary structure, base pair geometry or duplex base pairing to a substantial extent. The nick has, however, a noticeable impact on the local geometry at the nick site, indicated clearly by NMR analysis and reflected in the conformational parameters of the computed structure. The ^1H spectra also show much sharper resonances in the presence of K^+ indicating that conformational heterogeneity of DDSDPEG is reduced in the presence of potassium as compared to sodium or caesium ions. At the same time the ^1H resonances have longer T_1 times. This parameter is suggested as a sensitive gauge of stabilisation.

INTRODUCTION

There is an increasing interest in new forms of DNA oligonucleotides (1,2). This is mainly due to the view that oligonucleotide-based therapeutics may potentially lead to a new approach in drug design by targeting DNA-binding proteins, in addition to the well-established strategies of targeting RNA by an antisense approach and DNA by antigene and triplex approaches. In line with this new view, several covalent and non-covalent complexes of human topoisomerase I with a series of 22 bp DNA duplexes have recently been studied by X-ray analysis (3,4). An understanding of the biological features of these bioconjugates at the molecular level requires at least a detailed knowledge of the nicking mechanism and features affecting the stability of DNA oligonucleotides. A wealth of information concerning these topics is available. Conformational and thermodynamic consequences of the introduction of a nick in duplex DNA fragments were established (5), demonstrating that nicked fragments essentially form regular B-DNA duplexes with small local distortions around the nick. This view is strengthened by recent studies of polymorphism and dynamics of nicked DNA with nucleotide bridges (6–8). Two strategies to enhance the stability of nucleotide fragments against exonucleases (9,10) have been developed, namely covalent linking of the two strands by thymidylates or by non-nucleotide bridging (11–14) using polyethylene glycol. Few spectroscopic studies of the latter oligonucleotides have been performed (13,14).

Our interest in dumbbell nicked DNA is related to the problem of targeting topoisomerase I by the camptothecin family of drugs, which stabilise nicked reaction intermediates and thus inhibit the action of topoisomerase I on DNA relaxation (15,16).

The role of cations in stabilising the helix form of DNA has, until recently, been solely assigned to their charge, following the polyelectrolyte theory (17) of polynucleotide stabilisation by charged ions. One can anticipate that the cation radius, its concentration and the overall ionic strength of the solution may well be important variables, as shown recently (18–20). A well-established NMR tool for monitoring overall dynamics and domain-specific conformational changes is the relaxation behaviour of polynucleotides reflected in T_1 and T_2 values (21). These problems have recently attracted increasing interest in studies of DNA oligonucleotides (22–28).

The title-gapped nucleotide was synthesised as the structure shown in Scheme 1.

*To whom correspondence should be addressed at: Institute of Organic Chemistry, Polish Academy of Sciences, 01-224 Warszawa, Kasprzaka 44, Poland. Tel: +48 22 632 3221; Fax: +48 22 632 6681; Email: lkoz@ichf.edu.pl

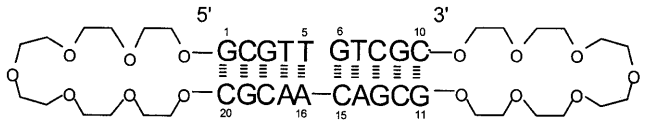

Scheme 1.

Our primary goal in this work was to measure and optimise the stability of the above dumbbell nicked DNA with respect to its utility as a substrate for the synthesis of bioconjugate-containing fragments of topoisomerase I at the T5 3′-OH site connected by a phosphodiester bond with Tyr723 4′-OH.

MATERIALS AND METHODS

Synthesis

Synthesis of the oligonucleotide was performed using an ABI 394 DNA synthesiser on a 1 μmol scale using phosphoramidite chemistry starting on T5. A, T, G and C phosphoramidites were purchased from ABI/Perkin Elmer (Warrington, UK). The PEG_6 spacer, 18-*O*-dimethoxytritylhexaethyleneglycol, 1-[(2-cyanoethyl)-(*N*,*N*-diisopropyl)]-phosphoramidite (Glen Research, Sterling, VA), was coupled with oligonucleotide during the normal synthesis cycle between G1-C20 and G11-C10. The oligonucleotide was purified by ion-exchange chromatography on a HiTrap™-Q column (Pharmacia Biotech) using gradient elution with ammonium bicarbonate solution (0.1–0.8 M) and desalted on Sephadex G-10.

Sample preparation

Samples for NMR measurements were prepared by dissolving the oligonucleotide in 38 mM K_3PO_4 or Na_2HPO_4 buffer containing sodium chloride (38 mM). The pH was adjusted to 7.0. Samples in H_2O contained 10% v/v D_2O. Samples examined in both H_2O and D_2O contained 0.9 mM oligonucleotide, except sample 2, which was 1.5 mM oligonucleotide. The concentration was measured by the UV absorption. TSP-d_4 was added to monitor the changes of chemical shifts at different temperatures. No EDTA was added to the samples, which were purified from paramagnetic impurities on a Chelex 100 column packing purchased from Bio-Rad Laboratories.

All samples measured were dissolved in 38 mM NaCl. The buffer concentration is given as counted on the phosphate ion. The sample and buffer concentrations were as follows: sample 1, 0.9 mM in 38 mM K_3PO_4, D_2O, pH 7.0, 152 mM in monovalent cation (114 mM in K^+); sample 2, 1.5 mM in 38 mM K_3PO_4, D_2O, pH 7.0, 152 mM in monovalent cation (114 mM in K^+); sample 3, lyophilised sample 1 and dissolved in deionized H_2O, pH 7.0, 152 mM in monovalent cation (114 mM in K^+); sample 4, 0.9 mM in 38 mM Na_2HPO_4 in H_2O, pH 6.0, 114 mM in monovalent cation (0 mM in K^+); sample 5, 0.9 mM in 38 mM Na_2HPO_4 + 38 mM K_3PO_4 in H_2O, pH 6.0 (Table 4) and pH 8.0, 228 mM in monovalent cation (114 mM in K^+); sample 6, 0.9 mM in 38 mM Na_2HPO_4 + 38 mM CsCl in H_2O, pH 6.0, 152 mM in monovalent cation (0 mM in K^+); sample 7, 0.9 mM in 38 mM Na_2HPO_4 + 38 mM CsCl + 38 mM KCl in H_2O, pH 6.0, 190 mM in monovalent cation (38 mM in K^+).

Melting temperature

The melting curve was determined by UV spectroscopy (Varian Cary 1E) on a 3 μM solution of oligonucleotide in 44 mM K_3PO_4 or Na_2HPO_4, sodium chloride buffer at pH 7.0 in the range 10–90°C.

NMR experiments

500 MHz ^{1}H NMR spectra were run using a 12 kHz spectral window (5 kHz for samples in D_2O) using the WATERGATE sequence (29) for water suppression for H_2O samples (with 1–5 ms soft pulses) and presaturation for samples in D_2O.

WATERGATE–NOESY spectra (30) in H_2O at 11°C were recorded on a Varian INOVA 500 MHz spectrometer using the States–TPPI (31) method to obtain phase-sensitive data, with 4096 data points in f_2 and 256 increments in f_1, z Gradients (20 Gauss/cm, 3 ms) were used to suppress spurious magnetisation. An 8 s delay before each scan was used and 16 scans were averaged. Spectra were apodised in both dimensions using a cosine bell. Linear prediction was applied in the f_1 dimension to extend the data over 512 complex data points and spectra were transformed into 4096 and 2048 points in f_2 and f_1, respectively.

NOESY spectra in D_2O were acquired with phosphorous decoupling in both dimensions and using low power presaturation of the residual HDO signal for 1.5 s. The spectral width in both dimensions was 5000 Hz, with 0.841 s acquisition time, 64 transients per 384 increments. To minimise artefacts coming from zero quantum coherences we used the known procedure of randomising the mixing times in the range of ±10 ms. The random changes were applied after each pass through the complete phase cycle (32).

E.COSY spectra (33) were acquired with and without phosphorous decoupling in both dimensions and using low power presaturation of the residual HDO signal for 1.2 s. The *J*-scaling with factor of 2 was applied to improve resolution. The spectral width in both dimensions was 3400 Hz, with 1.2 s acquisition time, 312 transients per 512 increments. The data were acquired using 8k complex points in the f_2 dimension (zero filled to 16k). Processing was performed on 2k complex points in f_1, linear predicted and zero filled to 4k.

TOCSY spectra (34) were acquired in phase-sensitive mode with a 5000 Hz spectral window in both dimensions, 1024 data points (zero filled to 2048), 16 transients per 256 increments (linear predicted to 1024 with zero filling to 2048) and relaxation delays of 1.5 s. Isotropic mixing times for TOCSY spectra ranged from 0.01 to 0.12 s and 8 kHz spin lock field was applied.

Longitudinal proton relaxation rates were measured by means of the standard inversion–recovery technique implemented in Varian software. Twelve recovery times from 0.1 to 12.5 s were used after the inverting pulse with a relaxation delay of 25 s and eight scans per experiment. The experimental intensities were fitted to an exponential equation yielding T_1 values with an error of less than ±0.1%.

The HMQC ^{1}H–^{31}P experiment (35,36) was performed in phase-sensitive mode (37) with 2048 × 128 points, and optimised for a ^{1}H–^{31}P coupling constant of 8 Hz; 192 scans were acquired and the spectral widths were 5000 and 6400 Hz in the ^{1}H and ^{31}P dimensions, respectively. The data were zero filled

to 2k × 1k with a π/2 shifted square sine bell window function in both dimensions.

The backbone torsion angles β and ε were determined through the measured *J*-couplings ^3J(C4′P) from heteronuclear single quantum coherence (HSQC) experiment (38). The gradient selected version of States–TTPI phase-sensitive HSQC with sensitivity enhancement was used. 800 scans for each of 256 increments were acquired and the spectral widths were 10 and 11 p.p.m. in the ^{1}H and ^{13}C dimensions, respectively. Zero filling corrections were applied in both dimensions to generate an 8k × 0.5k data matrix.

Cross-peaks in all of the NOESY spectra measured with short mixing times of 50, 75, 100 and 150 ms at 11 (H_2O) and 27°C (D_2O) were integrated using Felix. The peak intensities were all referenced to averaged volumes of C-H5, H6 cross-peaks over three non-overlapped cytidine units that had marginal volume variation.

Refinement of the calculated structure

Structural refinements were carried out using both energy-minimised A- and B-DNA as initial models to ensure the structures converge to the global minimum. Molecular mechanics calculations were carried out using the Amber force field (39) and the Discover_3 module from the software package Insight II version 98 (MSI). Electrostatic charges on DNA were taken from the Amber force field with reduced phosphate charges. The partial atomic charges for the PEG linkers were calculated by a semi-empirical SCF-MO calculation using the AM1 Hamiltonian and the module Mopac (Insight II). A distance-dependent dielectric constant value of 4.0 was used to mimic the bulk solvent effects, and a cutoff value of 30 Å was chosen to calculate all non-bonded interactions in the system.

Standard A- and B-DNA decamers with the nick at T5–G6 were built using the Biopolymer module, then PEG linkers were constructed using the Builder module and combined with DNA molecules using the Docking program (Insight II package). Preliminary molecular mechanics calculations were next performed for each structure to remove all strains, especially from PEG linkers. The calculations consisted of three steps: 2000 steps of energy minimisation using conjugate gradient algorithm, 50 ps molecular dynamics with 0.5 fs time steps at 300 K and, finally, energy minimisation by conjugate gradient until the energy gradient was <0.001 kcal/mol/Å. During these calculations positions of all atoms originated from DNA were kept fixed.

NOE-derived distance restraints

Distance restraints were obtained from quantitative analysis of NOE cross-peaks using an iterative relaxation matrix approach (IRMA) (40) implemented in module NMRchitect (Insight II). A total of 285 NOE-derived distance restraints were collected, 16 of which are interstrand (each base pair giving at least one interstrand NOE contact). In addition, crystallographic data were used to set up distance and angle restraints for hydrogen bonds in G-C and A-T base pairs for maintaining the Watson–Crick hydrogen bonding scheme between complementary base pairs (41). For G-C base pairs, distance constraints were set to 2.81 Å ≤ d(GO6, CN4) ≤ 3.01 Å; 2.85 Å ≤ d(GN1, CN3) ≤ 3.05 Å and 2.76 Å ≤ d(GN2, CO2) ≤ 2.96 Å. For A-T base pairs, distance restraints were set to 2.72 Å ≤ d(AN1, TN3) < 2.92 Å and 2.85 Å ≤ d(AN6, TO4) ≤ 3.05 Å. The atom hydrogen bond angles were set to 170–190°. The hydrogen bond restraints were used for all non-peripheral base pairs for which we can observe interstrand NOE cross-peaks.

Four to six cycles of IRMA iteration, including 50 ps of restrained molecular dynamics (rMD), were necessary to reach convergence as inspected by analysis of R-factors described in IRMA/NMRchitect module. The structures from the last IRMA cycles were further refined by introduction of torsion angle constraints and subsequent calculations using simulated annealing protocol. The majority of torsion angle restraints were obtained from analysis of coupling constants ^3J(H,H) and ^3J(C,P). The coupling constants ^3J(1′2′), ^3J(1′2″),^3J(2′3′) and ^3J(2″3′) were interpreted in terms of pseudorotation phase angles (P) and puckering amplitudes (Φ) with the aid of the program PSEUROT 6.2 (42). The backbone torsion angles β and ε were derived from ^3JC4′,P heteronuclear coupling constants. Right-handed α, γ and ζ backbone torsion angle restraints were also incorporated to maintain right-handedness, and to eliminate structural artefacts during the high temperature period. The torsion angle bonds were as follows: –90° < α < –30°, 30° < γ < 90° and 150° < ζ < 315°. A force constant of 40 kcal/mol/Å was set for NOE-distance restraints, 10 kcal/mol/Å for distance restraints derived from overlapping or poorly recorded NOE cross-peaks, 7 kcal/mol/Å for hydrogen bond constraints, 90 kcal/mol/rad for sugar and backbone β and ε torsion angle restraints and 8 kcal/mol/rad for backbone α, γ and ζ torsion angle restraints.

The protocol used for the rMD simulations is as follows: the system was heated from 0 to 700 K in the first 10 ps and 0.5 fs time steps whereby the restraint distance and angle force constants were scaled from 0.01 to 3. In the next 10 ps the system was equilibrated at 700 K and next during 20 ps gradually cooled to 300 K with force constants also gradually scaled down to 1. The system was kept in this condition for a further 100 ps and the collection of rMD structures was started after 50 ps with 1 ps intervals. A total of 50 structures was collected for each rMD run. The refined structures were obtained by coordinate averaging of the rMD structures after each rMD run. Structural artefacts of the averaged structure were removed by a 500 step restrained energy minimisation (rEM) process using steepest descent, followed by conjugate gradient minimisation until the energy gradient norm difference between successive steps was <0.0001 kcal/mol/Å. The final model was then generated by coordinate averaging of all refined rMD structures generated from A- and B-DNA initial models. The rEM process was performed to remove averaging artefacts followed by the 350 ps rMD run at 300 K with collection of 350 structures every 1 ps and rEM energy minimisation as above. The best 30 structures were selected on the basis of total energies.

The refinement protocol used in this work apparently results in no violation of the experimental restraints along the nick motif. However, a large twist (Ω angle) is observed in calculated structure at the nick motif, T5-A16/G6-C15 (see below). While the conservation of the experimental restraints cannot be sufficient evidence that this is not a calculation artefact of the protocol, nevertheless the analysis of the short time MD snapshots (~100 ps) reveals that, when the Ω is large, the EM results in low energy conformer.

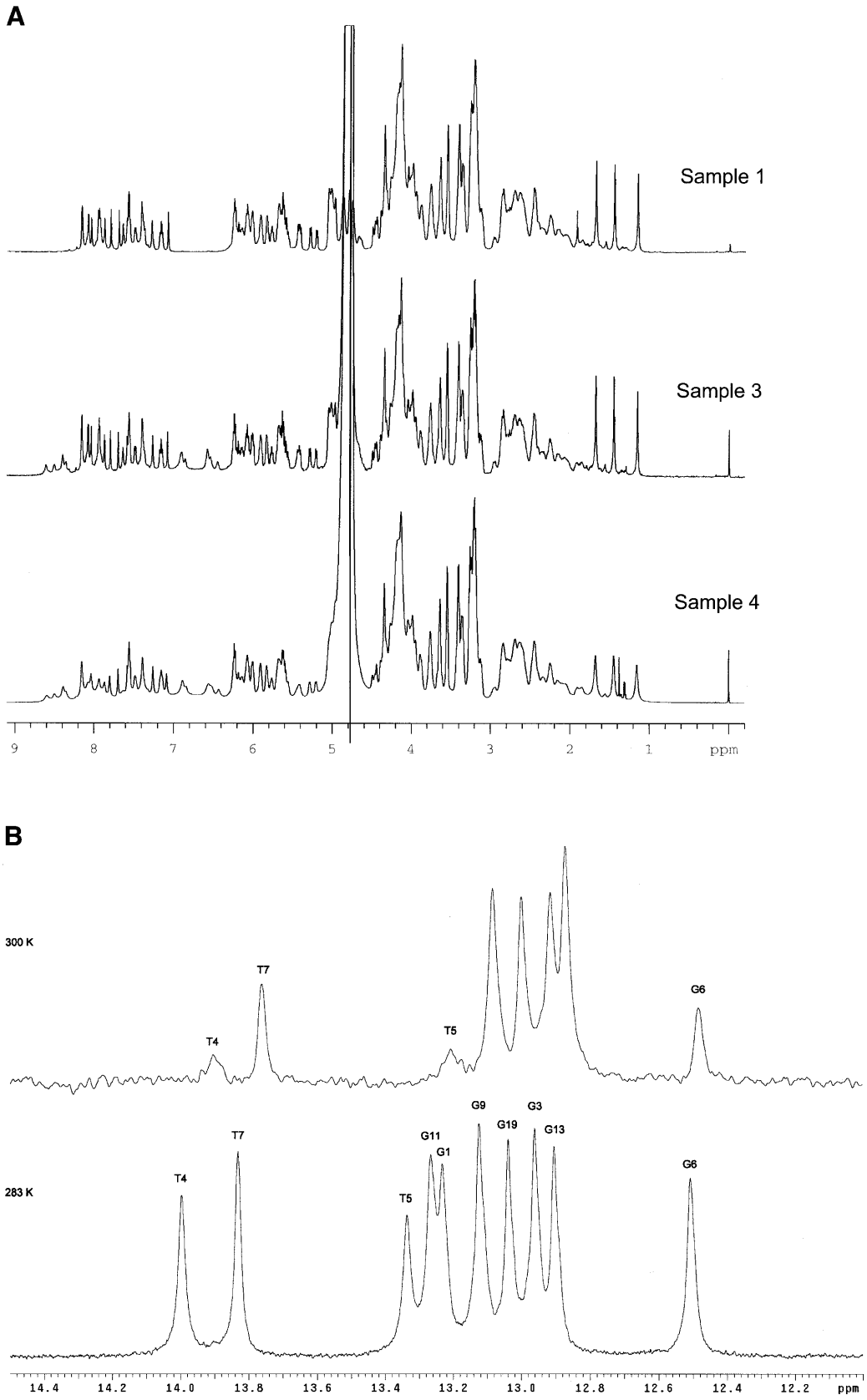

Figure 1. (**A**) ^{1}H 1-D spectrum of DDSDPEG in samples 1, 3 and 4 at 27°C. (**B**) NH region expansion of sample 3.

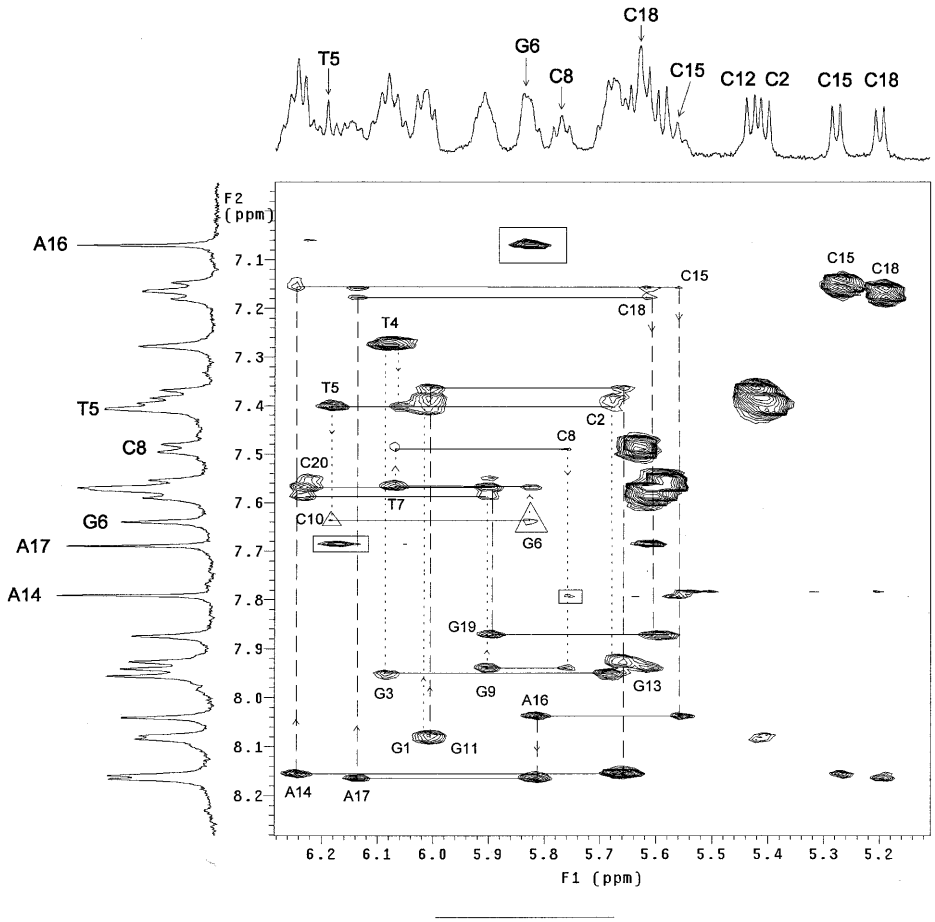

Figure 2. Expansion of NOESY spectrum, 50 ms mixing time, sample 1, 27°C, showing the region of H6/H8–H1′/H5 interactions. Cross-peaks in triangles indicate interactions across the nick (T5–G6), and cross-peaks in squares show the interactions of A H2 protons across the nick to the opposite strand.

RESULTS AND DISCUSSION

Assignment of the NMR signals at pH 7

Figure 1A shows the ^{1}H NMR spectra of the nicked double-stranded decamer in D_2O and H_2O with different buffers to show the influence of the cation on signal line-widths (see below). For sample 3 cited in Figure 1A, the expansion of imine protons region is shown in Figure 1B to evidence the base pairing. Assignment of the resonances was performed using established procedures (43,44). A portion of the 50 ms mixing time NOESY spectrum, showing the sequential assignments of H6/H8 versus H1′ resonances of the decamer, is shown in Figure 2. The other resonances, i.e. 2′, 2″, 3′ and 4′, have been assigned by combined analysis of NOESY and TOCSY (20, 50 and 80 ms mixing time) spectra (see Supplementary Material, Fig. S1). The assignment of 5′ and 5″ resonances was not attempted due to poor spectral dispersion of that region. The resonances of the PEG linker appear in the 3.1–4.0 p.p.m. region in several groups, and are much more dispersed than the corresponding resonances in the parent uncomplexed 21-[7] crown ether (45). The parent crown ether is known to complex both potassium and sodium ions with log K for binding of 4.22 and 1.73, respectively (46). However, from the invariance of all resonances belonging to the PEG linker of dumbbell double-stranded DNA decamer tethered with a PEG linker (DDSDPEG) in all experiments performed in this study with Na^+, K^+ and Cs^+ ions it may be suggested that none of them forms complexes with the tether part. This conclusion is strengthened by the lack of dependence of ^{1}H relaxation times of the PEG_6 linker on cations, noted in Table 1. It seems likely that the tether is restricted to an irregular and stiff shape too flat to accommodate any of these ions and does not act as a chelating crown ether as shown in the calculated structure. The exchangeable proton resonances of cytidine NH_2 groups are shown in Figure 1A in the 6.4–6.8 p.p.m. region for non-hydrogen-bonded NH^F, and the 8.0–8.4 p.p.m. region for hydrogen-bonded NH^B protons, respectively. The NH resonances of thymidines and guanosines appear in the 12–14 p.p.m. region as broadened signals; Figure 1B, some of them (T4, T5, G6, G1 and G11) showing exchange cross-peaks with H_2O even at 10°C. These are protons at the ends of strands or surrounding the nick which apparently are less strongly hydrogen bonded, possibly due to fraying. The assignment of these resonances is straightforward by established strategies (43,44) using intraresidue H5-NH^F and H5-NH^B dipolar contacts in cytidines and the interresidue intrapair contacts C,NH^B-G/T,NH.

Table 1. ^{1}H T_1 (s ± 0.02 s) relaxation times in the PEG_6 tethered decamer measured in Na_2HPO_4 (sample 4) and Na_2HPO_4 + K_3PO_4 buffer (sample 5, in parentheses) in H_2O at pH 6.0, 30°C[a]

	5′-G1	C2	G3	T4	T5	G6	T7	C8	G9	C10-3′
H6/H8	0.32(0.57)	0.45(0.65)	0.30(0.42)	0.54(0.77)	0.42(0.65)	0.48(0.68)	0.62(0.78)	0.40(0.63)	0.31(0.80)	0.63(0.80)
H1′	0.68(0.92)				0.54(0.84)	0.48(0.74)		0.47(0.76)		0.67(0.85)
CH_3				0.38(0.68)	0.32(0.60)		0.41(0.68)			
H5		(0.56)						(0.82)		0.62(0.86)
NH	0.41(0.53)		0.45(0.66)						0.47(0.57)	
NH		0.45(0.53)						0.51(0.53)		0.41(0.53)
H5	0.63(0.86)		0.41(0.70)			0.36(0.61)			(0.56)	
H2				0.50(0.80)	0.42(0.72)		0.33(0.63)			
H1′	0.64(0.85)			(0.77)	(0.76)	(0.70)				0.68(0.92)
H6/H8	0.61(0.78)	0.35(0.60)	0.42(0.63)	0.38(0.63)	0.31(0.54)	0.42(0.63)	0.38(0.63)	0.32(0.49)	(0.65)	0.32(0.57)
	3′-C20	G19	C18	A17	A16	C15	A14	G13	C12	G11-5′

[a]PEG linker resonances do not show differences in shape in both solutions and T_1 relaxation times are very close and on average equal 0.58 and 0.62 s, respectively.

NMR spectral parameters at pH 7.0

^{1}H NMR chemical shifts. ^{1}H NMR chemical shift data at 27°C are given in Table S1 (see Supplementary Material). The dispersion of chemical shifts of the deoxyribose protons is regular and characteristic for B-DNA structure with exceptions that may be attributed to the presence of the nick. In general, low frequency shifts are observed for protons at the nick. The H8 proton of G6 resonates at the lowest frequency of all the guanosyl H8 protons and, in addition, is broader than the others. Similarly, the H3′ protons of G6 and T5 show resonances ~0.2 p.p.m. shifted to lower frequencies than all other H3′ protons. The chemical shifts of H2′ and H2″ of G5 and G6 coincide at 27°C.

^{31}P NMR parameters. The ^{31}P chemical shift dispersion is very low, 0.7 p.p.m., (Table S1) characteristic for right-handed helices (47,48). The resonances of internucleotide ^{31}P atoms resonate at about –0.1 to –0.7 p.p.m. Two resonances fall outside this range, to higher frequencies, i.e. 0.85 and 0.18 p.p.m., for PEGpG1/G11 and PEGpC10/C20, which are the phosphates flanking the PEG linkers from the 5′ and 3′ sides, respectively. This high frequency shift is linked to the presence of one atom less in the γ position in PEG with respect to the deoxyribose unit. The assignment of ^{31}P resonances was aided by an HMQC spectrum, which shows very sharp correlation peaks for terminal phosphorous atoms linked to the PEG tether and broader cross-peaks for the other phosphorous atoms, due to scalar coupling with H3′ and H4′ protons. The ^{31}P resonances of G1pC2 and G11pC12 resonate at the lowest frequencies whereas G9pC10 and G19pC20 appear at the highest frequencies. ^3J(P,H) vicinal coupling constants, which are useful to define tertiary structure (49,50), could not be measured due to low spectral resolution [^3J(P,C) coupling constants are listed in Table S2 (see Supplementary Material)].

Vicinal coupling constants. ^3J(H1′,H2′), ^3J(H1′,H2″), ^3J(H3′,H2′) and ^3J(H3′,H2″) values are listed in Table S2 (see also Supplementary Material, Fig. S2). Strong overlap of signals due to G1, G11 and C10, C20 did not allow evaluation of the above mentioned vicinal couplings separately. They are assumed to be equal as given in Table S2. In general, the couplings do not differ for both strands indicating the regular B-DNA structure of all pairs with ^3J(H1′,H2′) values ~8–10 Hz and ^3J(H1′,H2″) values ~5–6 Hz indicating the predominance of a South deoxysugar pucker for all pairs in both strands, characteristic for B-DNA.

^1H T_1 non-selective relaxation time measurements. It is well known that non-selective ^{1}H T_1 relaxation times tend to be uniform in large biomolecules due to spin diffusion. Therefore, the aim of these experiments was to compare the T_1 values between the different samples rather than within the same sample. Thus, we have measured the non-selective ^{1}H T_1 relaxation times to check for possible differences in mobility along both strands. Different samples were examined to check for the effect of cations, ionic strength and pH on DNA structure and stabilisation. Some values are presented in Tables 1 and S2. The T_1 values of aromatic bases are uniform along both strands and are of the order of 1.5 s with the exception of H2 protons of adenosines, which relax slowly (4 s) due to poor dipolar contacts inside the bottom of the groove. Methyl groups of thymidines have, on average, the same relaxation times as aromatic H8/H6 protons or H1′ of deoxyribose protons.

For the nucleotide resonances, T_1 values are longer for the D_2O sample. This is hardly surprising, since it is well established that T_1 values decrease in H_2O due to efficient through-space relaxation and proton exchange with water (27), and also to the fact that nucleotide residues are in more rigid positions in D_2O, because of stronger hydrogen bonding, base–base stacking and ion binding than in H_2O (23). T_2 values are therefore also longer in D_2O, manifest as sharp lines (half-width of

methyl resonances ~3.5 and 2 Hz for AH2s, see projections in Fig. 2). For similar reasons, T_1 values decrease as the pH is lowered from 8.0 to 6.0.

In all samples studied, both T_1 and T_2 times were longer when K^+ ions were present than when only Na^+ and/or Cs^+ ions were present.

The duplex stability dependence on the pH, ionic strength and the cation

The duplex stability has been checked in solutions of a range of ionic strength, pH values and cations. Representative spectra are given in Figure 1 which compares the solutions 1, 3 and 4. We have used the half-width of methyl resonances as a measure of relative structure stability in different solutions. These half-widths are given for some of the measured samples in Table 2. Also noteworthy is the fact that a change from D_2O to H_2O solution (sample 1 versus 3) does not alter the signal half-width, although the T_1 values are shorter in H_2O. This is not unexpected, as the spin reservoir is filled with protons, which facilitate dipol–dipol relaxation (see above). The dependence on the pH is obvious, the higher pH gives the smaller line-width. This effect can be substantially enhanced if potassium buffer is used instead of sodium buffer at similar overall ionic strength; this results in better stabilisation of the duplex manifest in signal narrowing. The effect is suggested to result from stronger potassium binding with respect to other monovalent cations. This selective ion stabilisation effect is further confirmed by the fact that an increase in concentration in other monovalent cations, Na^+ or Cs^+, does not result in signal narrowing. The comparison of samples 6 and 7 is particularly noteworthy. The signals are substantially narrowed, by ~40%, in sample 7 after addition of 38 mM of KCl to sample 6. In comparison, the addition of the same amount of NaCl to sample 2 results in only ~15% decrease of line-width, attributed to higher cation concentration. It is also worth pointing out that the enhanced duplex stability by potassium is not resulting from the complex formation by the PEG_6 tether since the T_1 relaxation of this part of the molecule, or the shape of the signals, does not depend on the cation.

The rotational correlation time for the decamer can be assumed to be 3–7 ns, similar to values previously measured for the same size of DNA oligomers (22,26–28) Thus, the molecule is in the slow tumbling regime at the frequency used ($\omega\tau_c \approx 15$). However, as T_1 and T_2 behave in the same manner, then relaxation properties must be controlled by local motions (27). A reduction in local motion (i.e. a more stabilised structure) will have longer relaxation times for both T_1 and T_2. We therefore conclude that the longer relaxation times with K^+ indicate a strengthening of intramolecular constraints, mainly of ion binding and base pairing.

Protons of the PEG_6 linker have the shortest relaxation times of all protons in the molecule, ~0.6 s in all cases. This value is characteristic of mobility greater than that of the nucleotide stem. It therefore suggests that the linker is less constrained than the stem, which is not unexpected. It can, however, be reasoned that the PEG_6 linker restricts the mobility of the two pentamers of the gapped strand and, in effect, results in enhanced stability of the whole molecule. Relaxation times in the linker change very little on addition of K^+ (Table 1), confirming the conclusions made above that the linker does not chelate metal ions, unlike the parent crown ether.

Table 2. Methyl signal line-width, $\nu_{1/2}$, (Hz) in different solutions of decamer[a]

Sample	Monovalent cation	[K+] (mM)	pH	$\nu_{1/2}$ T5	T4	T7
1	152	114	7.0	6.5	5.6	5.9
2	152[b]	114	7.0	7.8	4.3	6.3
	190[c]	114	7.0	6.7	3.8	5.3
3	152	114	7.0	4.9	4.3	4.5
4	118	0	6.0	15.0	9.0	11.1
5	228	114	6.0	7.0	4.2	5.2
6	152	0	6.0	21.1	17.0	19.7
7	190[d]	38	6.0	13.0	10.5	12.0

[a]The line-width of TSP signal is in the range of 0.8–1.2 Hz for all studied samples. Phosphate ion concentration is 38 mM in all samples except 5, which is 76 mM in phosphate ion. Samples 1–3 are in D_2O and 4–7 in H_2O/D_2O, 9:1 v/v.
[b]Original sample 2.
[c]Sample 2 with 38 mM of NaCl added.
[d]Sample 6 with 38 mM of KCl added.

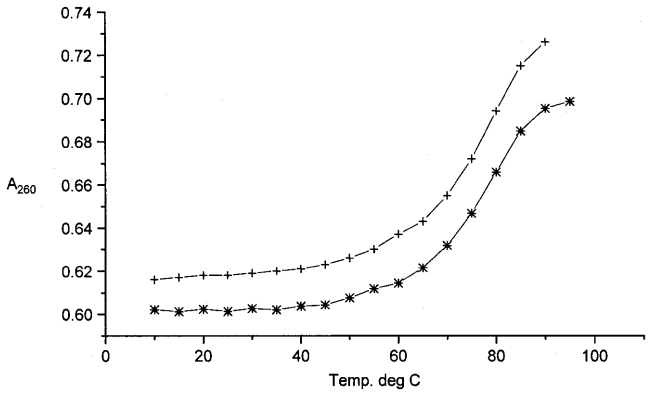

Figure 3. Melting temperature curves for the nicked decamer in Na^+ (*) and K^+ (+) buffers.

Concentration and temperature effects

Samples used for structural elucidations were 0.9 mM in DNA at a low salt concentration of 38 mM both in D_2O and in D_2O/H_2O (1:9 v/v). Doubling the DNA concentration did not result in chemical shift changes but led to partial precipitation of the solute, i.e. the solubility of the tethered DNA decamer is limited to ~1.5 mM.

The hexaethylene bridge, PEG_6, used in this study, provides very high temperature stability of the nicked decamer, $T_m = 80°C$ (Fig. 3). There is negligible difference in T_m values between samples measured in potassium and sodium buffers, somewhat at variance with the conclusion from relaxation studies. This is not unexpected, however, since the melting temperature is the cooperative property involving concerted dynamic behaviour

of several base pairs whereas the line-widths or T_1 values reflect mainly local dynamic properties of individual base pairs. Therefore, it is much easier to observe these changes on that level, especially on short oligonucleotides, in addition, tethered at both ends. Furthermore, the UV experiment was performed on samples of three orders of magnitude lower concentration than the NMR experiment and hence small changes in T_m may not manifest. Nevertheless, the measured melting temperature is even higher than that obtained with the longer oligonucleotides studied by Gao *et al.* (13) by using triethylene glycol bridges or pentathymidylate (T_5) bridges, or the PEG_6 or PEG_7 bridged hairpins of hexamer duplexes studied by Rumney and Kool (51). The melting temperature is comparable only with that of a 20mer ligated pentathymidylate bridged duplex (T_m = 82.5°C) or a ligated PEG_3 tethered dodecamer duplex (T_m = 93°C). Unligated duplexes corresponding to the above have T_m = 61.5 and 58.5°C, respectively, whereas the natural, unbridged 20mer duplex has T_m = 62°C. We attribute the duplex stability to the stiffness introduced by the linker at both ends of the stem. Corresponding to the high thermal stability, the one-dimensional (1-D) spectrum of the studied decamer shows only one set of sharp signals, thus proving that there is no spectral process underlying to indicate any intermolecular dynamics of the solute. Figure S3 (see Supplementary Material) shows spectra of the decamer at 10 and 27°C which confirm the above conclusion. Spectra recorded in D_2O/H_2O (1:9) at different temperatures show negligible shifts of exchangeable protons but NHs of T4,T5 and G6 sharpen at 11°C. The broadening of these NHs can be considered as an indication of mobility at the nick. However, the uniform values of T_1 in both strands, the negligible temperature effect in the 1-D spectrum and the observation of interstrand NOEs from adenine H2 to H1′ of the 3′ side partner, as discussed below, do not justify any suggestion of extensive rotational freedom between A16 and C15. The only consistent trend observed around the nick is the low frequency shift of NHs and H3′ and H4′ of T5 and G6. This, however, can be assigned to fraying of both ends around the nick (rather than rotational mobility) as a low frequency shift is usually observed upon melting of duplexes. It is also possible that low-frequency shifts can be caused by bending of the whole structure, which would result in nucleotides around the nick getting out of the deshielding plane of adjacent stacked aromatic rings.

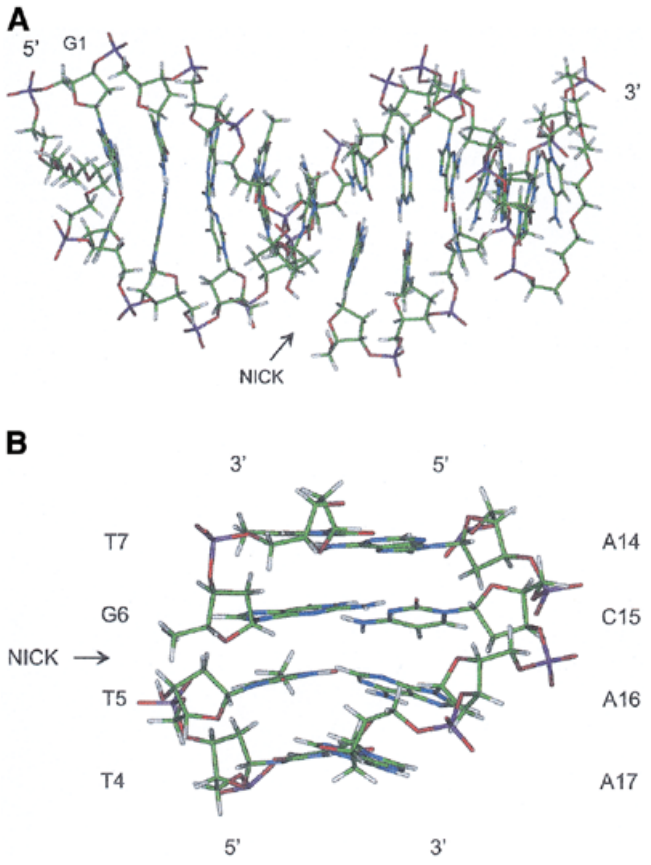

Figure 4. (**A**) Minor groove side view of the computed average structure of the nicked decamer and (**B**) minor groove side view of the nick flanked with 2 bp.

Tertiary structure of theoretical decamer, effect of a nick on duplex structure

The 3-D structures of the nicked decamer with a PEG_6 tether at each end were calculated with a set of 285 NOEs and 124 coupling constants as structural restraints, supplemented by 54 hydrogen bonds restraints and 51 backbone torsions. The low r.m.s.d. fluctuations from average structure taken over the entire trajectory of 350 ps rMD indicate sufficient stability of used protocol (Fig. S4). The 30 lowest energy structures were sampled pretty uniformly over the trajectory, which, we believe, gave good representation of the minimum energy structures used next for the calculation of the average conformer. One should keep in mind, however, that these structures may not be sufficiently representative for the room temperature ensemble. The average structure is depicted in Figure 4A and the structural statistics are given in Table 3. Structural parameters calculated for the structures using ancillary programs CURVES (52) and PSEUROT are given in Tables 4–6. The structure of the ribose ring including pseudorotation is well determined using coupling constants and intraresidue H6/H8 to H2′/H2″/H3′ NOEs. The local helical parameters and geometry of base pairs are, in contrast, underdetermined by NOE data since the interresidue proton distances are dependent on several conformational parameters which can be changed in a concerted manner (53,54). In the following we discuss the tertiary structure details, deduced from experimental constraints, and their relation to computed parameters, as determined by a molecular modelling.

Figure 2 shows the H6/H8–H1′/H5 region expansion of a 2-D NOESY spectrum at 50 ms mixing time at 10°C. This spectrum shows several interesting features. It primarily evidences good stability of the base pairs at the nick T5–G6, because cross-peaks (triangles) establish a connection between the two units despite the fact that there is no covalent linkage between them. Secondly, adenine H2 protons show sequential cross-peaks to H1′ protons of the 5′ side partner and interstrand cross-peaks to the H1′ proton of the i + 1 partner on the 3′ side (squares). The latter cross-peaks, such as A16,H2-G6,H1′, are some of the strongest in this region of the spectrum and are observed through the nick. The dipolar contacts at the nick site are characteristic of a covalently bonded duplex. Not shown in this spectrum are empty regions around the diagonal in the 2-D

Table 3. Structural statistics of the computed theoretical decamer

No. of distance restraints	285			
Interstrand	16			
No. of torsion angle restraints	175			
Derived from coupling constants	124			
No. of hydrogen-bond restraints	54			
Experimental restraints violated >0.2 Å				
T5,H4′-T5,H6	+0.48 ± 0.02			
T7,H4′-T7,H6	+0.56 ± 0.01			
G9,H1′-G9,H8	+0.29 ± 0.01			
G13,H4′-G13,H2″	+0.36 ± 0.01			
A17,H4′-A17,H2″	+0.30 ± 0.01			
Energy[a,b] (kcal/mol)				
E_{tot}	47.59 ± 1.68			
E_{vdw}	–210.7 ± 4.2			
$E_{constraint}$	94.3 ± 3.4			
R-factor	0.41 ± 0.01			
R(1/6)-factor	0.0045 ± 0.0001			
Atomic r.m.s.d.[b] (Å)				
All molecule	1.22 ± 0.51			
With no PEG	0.94 ± 0.54			
For each base	G1	0.93 ± 0.53	C20	0.71 ± 0.39
	C2	0.85 ± 0.50	G19	0.53 ± 0.27
	G3	1.02 ± 0.62	C18	0.43 ± 0.25
	T4	1.34 ± 0.76	A17	0.40 ± 0.25
	T5	1.55 ± 0.89	A16	0.62 ± 0.38
	G6	0.72 ± 0.43	C15	0.83 ± 0.52
	T7	0.52 ± 0.19	A14	0.76 ± 0.45
	C8	0.49 ± 0.26	G13	0.94 ± 0.53
	G9	0.60 ± 0.34	C12	1.48 ± 0.91
	C10	0.79 ± 0.46	G11	1.91 ± 1.04

[a]Energy was calculated using the Amber force field with the Discover program from Insight 98 (MSI).
[b]Average parameters for the 30 lowest energy refined structures (± standard deviations).

NOESY spectrum of H1′ and H8/H6 resonances, giving evidence of absence of stacking of duplexes (6). Finally, the relative intensities of sequential intra- and interresidue dipolar contacts due to H8/H6–H2′/H2″ are characteristic for B-DNA. The same feature is also observed in the spectral region of H8/H6–H1′ in Figure 2. The above observations find relevant reflection in the computed structural parameters given in Table 4. The χ angle is uniform in all units (except G19) and characteristic for the *anti* conformation of the glycosidic bond. The ribose ring pucker parameters are characteristic for B-DNA type, the pseudo-rotation phase P being in the range of 144–180° and the amplitude Φ between 30 and 42°. Three exceptions are observed, namely, one at the nick, (P = 45°, C4′-exo, N-type pucker of G6) which may be induced by the nick and distorted S-type pucker conformations of C10 and C20, which could be induced by PEG conformational requirements.

We have also observed several long-range effects, which can influence global helical parameters. As mentioned earlier, the sequence of intensities of cross-peaks due to intra- and inter-strand contacts H8/H6–H2′ and H8/H6–H2″ follow a pattern characteristic for B-DNA. On the other hand, the interresidue sequential contacts of H8/H6–H1′ are, on average, longer in the nicked strand, ~4 Å, than in the unbroken strand, ~3.5 Å. In regular A- and B-DNA these distances are 4.0 and 2.8 Å, respectively (43). These results seem to indicate interresidue distances more characteristic for A-DNA in the nicked strand. The same trend is observed in restraints refined by the IRMA procedure during calculation of the structure and in comparison of

Table 4. Backbone and pseudorotation ring pucker parameters of calculated structure of nicked decamer[a]

Glycosidic and backbone torsions (deg)								Ribose ring parameters		
	C1′-N	P-O5′	O5′-C5′	C5′-C4′	C4′-C3′	C3′-O3′	O3′-P	Phase	Amplitude	Pucker
	χ	α	β	γ	δ	ε	ζ	P	Φ	
Scissile strand										
G1-5′	–113 ± 3	–76 ± 11	174 ± 5	59 ± 5	141 ± 1	–179 ± 2	–93 ± 2	163 ± 2	38 ± 1	C2′-endo(S)
C2	–116 ± 1	–78 ± 1	–175 ± 2	51 ± 1	132 ± 1	–158 ± 3	–157 ± 3	144 ± 1	42 ± 1	C1′-exo(S)
G3	–114 ± 4	–68 ± 1	150 ± 6	71 ± 3	142 ± 1	–177 ± 1	–87 ± 1	171 ± 1	37 ± 1	C2′-endo(S)
T4	–131 ± 5	–74 ± 2	170 ± 1	58 ± 1	116 ± 1	178 ± 2	–98 ± 3	118 ± 2	33 ± 1	C1′-exo(S)
T5-3′	–130 ± 3	–61 ± 8	174 ± 9	75 ± 11	125 ± 2			168 ± 3	33 ± 1	C2′-endo(S)
G6-5′	–157 ± 1			64 ± 2	86 ± 1	–178 ± 1	–72 ± 1	45 ± 2	35 ± 1	C4′-exo(N)
T7	–134 ± 1	–64 ± 1	179 ± 1	73 ± 1	128 ± 1	179 ± 1	–83 ± 1	180 ± 1	38 ± 1	C3′-exo(S)
C8	–129 ± 1	–76 ± 1	178 ± 1	48 ± 1	120 ± 1	178 ± 1	–91 ± 1	131 ± 1	33 ± 1	C1′-exo(S)
G9	–125 ± 1	–64 ± 1	179 ± 1	55 ± 1	132 ± 1	–178 ± 1	–100 ± 1	146 ± 1	36 ± 1	C2′-endo(S)
C10-3′	–135 ± 2	–69 ± 1	–179 ± 3	59 ± 5	98 ± 2	179 ± 2	–93 ± 2	82 ± 4	33 ± 1	O4′endo(S)
Non-scissile strand										
C20-3′	–119 ± 3	–71 ± 1	165 ± 2	64 ± 3	94 ± 3	–173 ± 18	–93 ± 20	77 ± 4	33 ± 1	O4′-endo(S)
G19	–85 ± 1	–66 ± 1	178 ± 2	64 ± 1	133 ± 1	–179 ± 2	–109 ± 2	155 ± 1	30 ± 1	C2′-endo(S)
C18	–136 ± 1	–72 ± 2	177 ± 1	54 ± 2	113 ± 1	–170 ± 1	–90 ± 1	104 ± 1	33 ± 1	O4′-endo(S)
A17	–124 ± 1	–65 ± 1	179 ± 2	68 ± 2	121 ± 2	–179 ± 1	–102 ± 2	131 ± 2	39 ± 1	C1′-exo(S)
A16	–105 ± 2	–62 ± 1	167 ± 1	64 ± 2	139 ± 2	169 ± 1	–94 ± 2	156 ± 2	39 ± 1	C2′-endo(S)
C15	–118 ± 3	–75 ± 5	171 ± 1	63 ± 2	120 ± 2	–179 ± 1	–91 ± 3	124 ± 2	32 ± 1	C1′-exo(S)
A14	–112 ± 2	–74 ± 5	–174 ± 1	50 ± 1	132 ± 2	–179 ± 2	–101 ± 2	144 ± 2	34 ± 1	C1′-exo(S)
G13	–131 ± 1	–70 ± 1	174 ± 1	61 ± 1	118 ± 1	178 ± 2	–99 ± 2	126 ± 1	40 ± 1	C1′-exo(S)
C12	–132 ± 1	–76 ± 1	–180 ± 2	54 ± 1	120 ± 1	–174 ± 2	–93 ± 1	124 ± 1	36 ± 1	C1′-exo(S)
G11-5′	–117 ± 3	–159 ± 90	–177 ± 11	119 ± 60	141 ± 3	–179 ± 2	–95 ± 1	163 ± 3	37 ± 1	C2′-endo(S)

[a]The backbone torsion definition in agreement with IUPAC recommendation. Average parameters for the 30 lowest energy refined structures (± standard deviations).

these distances in the final refined structure. Another unusual fact is the presence of interstrand contacts of adenine H2 protons to H1′ protons of the i + 1 partner at the 3′ side, of the type A16,H2-G6,H1′, which are characteristic of bent structures (43). In contrast to the above facts intraresidue scalar coupling pattern of ^{3}J(H1′,H2′) (~8–10 Hz) and ^{3}J(H1′,H2″) (~5–6 Hz) are characteristic of a B-DNA type duplex. However, the presence of the above contradictory local geometry distortions is not unexpected due to the presence of the three deforming motifs; i.e. two tethers at both ends and the nick. While the local geometry is changed, the concerted changes of several degrees of freedom leaves the global axis unaffected. This discussion finds its reflection in global conformational parameters found for computed structure shown in Figure 4 and listed in Tables 5 and 6. As shown in Figure 4A and B, the first two pairs and also those flanking the nick are substantially buckled as compared with the other pairs. The two base pairs flanking the nick are substantially twisted (Ω = 63°) as compared with the other interpair parameter; however, the average is 34° resulting in 10.6 bp/turn, again in agreement with standard B-DNA type. The plot of the Ω angle for the T5-A16/G6-C15 base pairs versus time of rMD shows that for early steps (up to 60 ps) the Ω angle remains at ~63°, and for the rest of the time starts to randomly adopt two separated values at ~63 and 39°, as is shown in Figure S4. However, the conformers with the Ω angle 63° usually have lower energy. This behaviour may be explained as being a force field derived artefact or as a normal behaviour of this type of DNA. However, more reliable and more representative as low energy conformers are the conformers with Ω angle equal to ~63°. Furthermore, as mentioned earlier, the refinement protocol results in no violation of experimental restraints at the nick motif, which gives further confidence in calculated structure.

CONCLUSIONS

We have determined the structure of a dumbbell DNA with a 10 base stem having a nick in the centre and hexaethylene glycol linkers at either side using NMR spectral parameters, i.e. chemical shifts of ^{1}H and ^{31}P, scalar vicinal (H, H) coupling constants, T_1 measurements and dipolar interactions to characterise the structure.

Table 5. Selected global Base pair–Axis and Base–Base parameters[a]

	Base pair–Axis		Base–Base	
	Inclin. (η)	Tip (θ)	Buckle (κ)	Opening (σ)
G1-C20	–4 ± 4	0 ± 4	–26 ± 4	–3 ± 3
C2-G19	–6 ± 5	10 ± 3	–20 ± 3	2 ± 1
G3-C18	–6 ± 5	–1 ± 2	15 ± 2	–8 ± 2
T4-A17	–10 ± 5	7 ± 3	3 ± 9	–5 ± 1
T5-A16	–6 ± 8	5 ± 2	1 ± 22	–2 ± 1
G6-C15	–8 ± 5	7 ± 4	–26 ± 3	5 ± 2
T7-A14	–9 ± 5	2 ± 2	–10 ± 1	–6 ± 1
C8-G13	–12 ± 5	2 ± 2	–2 ± 2	–6 ± 1
G9-C12	–16 ± 4	1 ± 2	–4 ± 3	–11 ± 1
C10-G11	–12 ± 4	2 ± 1	–10 ± 3	–4 ± 1

[a]Average parameters for the 30 lowest energy refined structures (± standard deviations) calculated with program CURVES.

Table 6. Selected global interbase pair parameters[a]

	Tilt (τ)	Roll (ρ)	Twist (Ω)
G1-C20/C2-G19	–4 ± 1	9 ± 3	33 ± 1
C2-G19/G3-C18	–2 ± 1	–11 ± 2	40 ± 1
G3-C18/T4-A17	–1 ± 2	9 ± 1	36 ± 2
T4-A17/T5-A16	2 ± 5	–6 ± 4	39 ± 2
T5-A16/G6-C15	11 ± 7	9 ± 4	63 ± 1
G6-C15/T7-A14	0 ± 1	8 ± 1	30 ± 1
T7-A14/C8-G13	–1 ± 2	9 ± 1	35 ± 1
C8-G13/G9-C12	–2 ± 1	5 ± 2	31 ± 1
G9-C12/C10-G11	7 ± 1	2 ± 3	37 ± 1

[a]Average parameters for the 30 lowest energy refined structures (± standard deviations) calculated with program CURVES.

It was found that the molecule in solution forms a stable duplex and, despite the nick, the structure is highly ordered with good stacking of the base pairs. The variable temperature studies revealed the remarkable stability of the duplex, which does not show evidence of internal mobility at pH 7 and low salt concentration. The stability is reflected in the high melting temperature, T_m = 80°C, which is comparable to the melting temperature of a ligated 20mer with a T_5 thymidylate bridge studied by Gao *et al.* (13). The stability of the stem duplex is enhanced by the rigid loops of hexaethylene glycol which hinder possible fraying of pentamers on the stem. It is concluded that this type of bridging may be especially efficient in restricting the dynamics in dumbbell nicked DNA oligomers. Therefore, this type of tether will be useful when investigating the nicked decamer duplex as a substrate for synthesis of bioconjugates containing a topoisomerase I fragment attached to the T5 3′-OH site by means of a phosphodiester bond with Tyr723 4′-OH.

Potassium ions are shown to stabilise the nicked DNA in the buffer concentration 152–190 mM. In our measurements we observed that T_1 measurements for both base and sugar protons increased in the solution containing potassium ions as compared to solutions containing sodium and caesium ions. T_1 measurements were shown to be a sensitive probe for monitoring changes in dynamics and base pairing stability.

The inspection of computed structure parameters and the nick motif suggests that its influence on the overall tertiary structure is not disturbing the base pair geometry and duplex base pairing to a substantial extent. The nick has, however, a noticeable impact on the local geometry at the nick site, indicated clearly by the NMR analysis and reflected in the conformational parameters of the computed structure.

SUPPLEMENTARY MATERIAL

Supplementary Material is available at NAR Online.

ACKNOWLEDGEMENT

We thank Dr W.Kozminski (Department of Chemistry, Warsaw University, Poland) for the new version of E.COSY pulse program.

REFERENCES

1. Wyatt,J.R., Vickers,T.A., Roberson,J.L., Buckheit,R.W., Klimkait,T., de Baets,E., Davis,P.W., Rayner,B., Imbach,J.L. and Ecker,D.J. (1994) Combinatorially selected guanosine-quartet structure is a potent inhibitor of human immunodeficiency virus envelope-mediated cell fusion. *Proc. Natl Acad. Sci. USA*, **91**, 1356–1360.
2. Lane,A.N. (1995) Determination of fast dynamics of nucleic acids by NMR. *Methods Enzymol.*, **261**, 413–435.
3. Redinbo,M.R., Stewart,L., Kuhn,P., Champoux,J.J. and Hol,W.G.J. (1998) Crystal structures of human topoisomerase I in covalent and noncovalent complexes with DNA. *Science*, **279**, 1504–1513.
4. Stewart,L., Redinbo,M.R., Qiu,X., Hol,W.G.J. and Champoux,J.J. (1998) A model for the mechanism of human topoisomerase I. *Science*, **279**, 1534–1541.
5. Pieters,J.M.L., Mans,R.M.W., van den Elst,H., van der Marel,G.A., van Boom,J.H. and Altona,C. (1989) Conformational and thermodynamic consequences of the introduction of a nick in duplexed DNA fragments: an NMR study augmented by biochemical experiments. *Nucleic Acids Res.*, **17**, 4551–4565.
6. Singh,S., Patel,P.K. and Hosur,R.V. (1997) Structural polymorphism and dynamism in the DNA segment GATCTTCCCCCCGGAA: NMR investigations of hairpin, dumbbell, nicked duplex, parallel strands, and i-motif. *Biochemistry*, **36**, 13214–13222.
7. Snowden-Ifft,E.A. and Wemmer,D.E. (1990) Characterization of the structure and melting of DNAs containing backbone nicks and gaps. *Biochemistry*, **29**, 6017–6025.
8. Rentzeperis,D., Ho,J. and Marky,L.A. (1993) Contribution of loops and nicks to the formation of DNA dumbbells: melting behavior and ligand binding. *Biochemistry*, **32**, 2564–2572.
9. Shaw,J.-P., Kent,K., Bird,J., Fishback,J. and Froehler,B. (1991) Modified deoxyoligonucleotides stable to exonuclease degradation in serum. *Nucleic Acids Res.*, **19**, 747–750.
10. Akhtar,S., Kole,R. and Juliano,R.L. (1991) Stability of antisense DNA oligodeoxynucleotide analogs in cellular extracts and sera. *Life Sci.*, **49**, 1793–1801.
11. Kool,E.T. (1991) Molecular recognition by circular oligonucleotides: increasing the selectivity of DNA binding. *J. Am. Chem. Soc.*, **113**, 6265–6266.

12. Rumney,S.,IV and Kool,E.T. (1992) DNA recognition by hybrid oligoether-oligodeoxynucleotide macrocycles. *Angew. Chem. Int. Ed. Engl.*, **31**, 1617–1619.
13. Gao,H., Chidambaram,N., Chen,B.C., Pelham,D.E., Patel,R., Yang,M., Zhou,L., Cook,A. and Cohen,J.S. (1994) Double-stranded cyclic oligonucleotides with non-nucleotide bridges. *Bioconjugate Chem.*, **5**, 445–453.
14. Durand,M., Chevrie,K., Chassignol,M., Thuong,N.T. and Maurizot,J.C. (1990) Circular dichroism studies of an oligodeoxyribonucleotide containing a hairpin loop made of a hexaethylene glycol chain: conformation and stability. *Nucleic Acids Res.*, **18**, 6353–6359.
15. Rivory,L.P. and Robert,J. (1995) Pharmacology of camptothecin and its derivatives. *Bull. Cancer*, **82**, 265–285.
16. Hsiang,Y.-H., Hertzberg,R., Hecht,S. and Liu,L.F. (1985) Camptothecin induces protein-linked DNA breaks via mammalian DNA topoisomerase I. *J. Biol. Chem.*, **260**, 14873–14878.
17. Manning,G.S. (1978) The molecular theory of polyelectrolyte solutions with applications to the electrostatic properties of polynucleotides. *Q. Rev. Biophys.*, **11**, 179–246.
18. Trend,B.L., Knoll,D.A., Ueno,M., Evans,D.F. and Bloomfield,V.A. (1990) Cation radius effects on the helix-coil transition of DNA. Cryptates and other large cations. *Biophys. J.*, **57**, 829–834.
19. Cerda,B.A. and Wesdemiotis,C. (1996) Li^+, Na^+, and K^+ binding to the DNA and RNA nucleobases. Bond energies and attachment sites from the dissociation of metal ion-bound heterodimers. *J. Am. Chem. Soc.*, **118**, 11884–11892.
20. Shui,X., Sines,C.C., McFail-Isom,L., VanDerveer,D. and Williams,L.D. (1998) The molecular theory of polyelectrolyte solutions with applications to the electrostatic properties of polynucleotides. *Biochemistry*, **37**, 16877–16887.
21. Lane,A.N. (1993) NMR studies of dynamics in nucleic acids. *Prog. Nucl. Magn. Reson. Spectrosc.*, **25**, 481–505.
22. Kojima,C., Ono,A., Kainosho,M. and James,T.L. (1998) DNA duplex dynamics: NMR relaxation studies of a decamer with uniformly 13-C labeled purine nucleotides. *J. Magn. Reson.*, **135**, 310–333.
23. Jing,N., Gao,X., Rando,R.F. and Hogan,M.E. (1997) Potassium-induced loop conformational transition of a potent anti-HIV oligonucleotide. *J. Biomol. Struct. Dyn.*, **15**, 573–585.
24. Lane,A.N. (1995) Determination of fast dynamics of nucleic acids by NMR. *Methods Enzymol.*, **261**, 413–435.
25. Eimer,W., Williamson,J.R., Boxer,S.G. and Pecora,R. (1990) Characterization of the overall and internal dynamics of short oligonucleotides by depolarized dynamic light scattering and NMR relaxation measurements. *Biochemistry*, **29**, 799–811.
26. Assa-Munt,N., Granot,J., Behling,R.W. and Kearns,D.R. (1984) ^{1}H NMR relaxation studies of the hydrogen-bonded imino protons of poly(dA-dT). *Biochemistry*, **23**, 944–955.
27. Feigon,J., Denny,W.A., Leupin,W. and Kearns,D.R. (1983) Proton nuclear magnetic resonance investigation of the conformation and dynamics in the synthetic deoxyribonucleic acid decamers d(ATATCGATAT) and d(ATATGCATAT). *Biochemistry*, **22**, 5930–5942.
28. Early,T.A., Kearns,D.R., Hillen,W. and Wells,R.D. (1980) A 300 MHz and 600 MHz proton NMR study of a 12 base pair restriction fragment: investigation of structure by relaxation measurements. *Nucleic Acids Res.*, **8**, 5795–5812.
29. Piotto,M., Saudek,V. and Sklenar,V. (1992) Gradient-tailored excitation for single-quantum NMR spectroscopy of aqueous solutions. *J. Biomol. NMR*, **2**, 661–665.
30. Jeener,J., Meier,B.H., Bachman,P. and Ernst,R.R. (1979) Investigation of exchange processes by two-dimensional NMR spectroscopy. *J. Chem. Phys.*, **71**, 4546–4553.
31. Bodenhausen,G., Kogler,H. and Ernst,R.R. (1984) Selection of coherence-transfer pathways in NMR pulse experiments. *J. Magn. Reson.*, **58**, 370–388.
32. Neuhaus,D. and Williamson,M. (1989) The nuclear overhauser effect in structural and conformational analysis, VCH, New York, pp. 285–288.
33. Griesinger,C., Sørensen,O.W. and Ernst,R.R. (1985) Two-dimensional correlation of connected NMR transitions. *J. Am. Chem. Soc.*, **107**, 6394–6396.
34. Griesinger,C., Otting,G., Wüthrich,K. and Ernst,R.R. (1988) Clean TOCSY for 1-H spin system identification in macromolecules. *J. Am. Chem. Soc.*, **110**, 7870–7872.
35. Bodenhausen,G. and Ruben,D.J., (1980) Natural abundance nitrogen-15 NMR by enhanced heteronuclear spectroscopy. *Chem. Phys. Lett.*, **69**, 185–189.
36. Bax,A. and Summers,M.F. (1986) 1-H and 13-C assignments from sensitivity-enhanced detection of heteronuclear multiple-bond connectivity by 2D multiple quantum NMR. *J. Am. Chem. Soc.*, **108**, 2093–2094.
37. States,D.J., Haberkorn,R.A. and Ruben,D.J. (1982) A two-dimensional nuclear Overhauser experiment with pure absorption phase in four quadrants. *J. Magn. Reson.*, **48**, 286–292.
38. Summers,M.F.J., Marzili,L.G. and Bax,A. (1986) Complete 1-H and 13-C assignments of Coenzyme B12 through the use of new two-dimensional NMR experiments. *J. Am. Chem. Soc.*, **108**, 4285–4294.
39. Weiner,S.J., Kollman,P.A., Nguyen,D.T. and Case,D.A. (1986) An all atom forcefield for simulations of proteins and nucleic acids. *J. Comp. Chem.*, **7**, 230–252.
40. Boelens,R., Koning,T.M.G., van der Marel,G.A., van Boom.,J.H. and Kaptein,R. (1989) Iterative procedure for structure determination from proton–proton NOEs using a full relaxation matrix approach. Application to a DNA octamer. *J. Magn. Reson.*, **82**, 290–308.
41. Lam,S.L. and Au-Yeung,S.C.F. (1997) Sequence-specific local structural variations in solution structures of $d(CGXX'CG)_2$ and $d(CAXX'TG)_2$ self-complementary deoxyribonucleic acids. *J. Mol. Biol.*, **266**, 745–760.
42. van Wijk,J., Huckriede,B.D., Ippel,J.H. and Altona,C. (1992) Furanose sugar conformations in DNA from NMR coupling constants. *Methods Enzymol.*, **211**, 286–306.
43. Goljer,I. and Bolton,P.H. (1994) In Croasmun,W.R. and Carlson,R.M.K. (eds), *Two-Dimensional NMR Spectroscopy: Applications for Chemists and Biochemists.* VCH Publishers, New York, pp. 699–740.
44. Bolton,P.H. (1990) A primer on isotopic labeling in NMR investigations of biopolymers. *Prog. Nucl. Magn. Reson. Spectrosc.*, **22**, 423–452.
45. Bradshaw,J.S., Baxter,S.L., Lamb,J.D., Izatt,R.M. and Christensen,J.J. (1981) Cation-complexing properties of synthetic macrocyclic polyether-diester ligands containing the furan, benzene, tetrahydrofuran, and thiophene subcyclic units. *J. Am. Chem. Soc.*, **103**, 1821–1827.
46. Izaat,R.M, Pawlak,K., Bradshaw,J.S. and Bruening,R.L. (1991) Thermodynamic and kinetic data for macrocycles interaction with cations and anions. *Chem. Rev.*, **91**, 1721–2085.
47. Varani ,G., Aboul-ela,F. and Allain,F.H.-T. (1996) NMR investigation of RNA structure. *Prog. Nucl. Magn. Reson. Spectrosc.*, **29**, 51–127.
48. Gorenstein,P.G. (1984) *Phosphorus-31, Principles and Applications.* Academic Press, New York.
49. Clark,G.R., Brown,D.G., Sanderson,M.R., Chwalinski,T., Neidle,S., Veal,J.M., Jones,R.L., Wilson,W.D., Zon,G., Garman,E. and Stuart,D.I. (1990) Crystal and solution structures of the oligonucleotide $d(ATGCGCAT)_2$: a combined X-ray and NMR study. *Nucleic Acids Res.*, **18**, 5521–5528.
50. Swaminathan,S., Ravishanker,G. and Beveridge,D.L. (1991) Molecular dynamics of B-DNA including Water and counterions: a 140-ps trajectory for d(CGCGAATTCGCG) based on the GROMOS force field. *J. Am. Chem. Soc.*, **113**, 5027–5040.
51. Rumney,S.,IV and Kool,E.T. (1995) Structural optimization of non-nucleotide loop replacements for duplex and triplex DNAs. *J. Am. Chem. Soc.*, **117**, 5635–5646.
52. Lavery,R. and Sklenar,H. (1988) The definition of generalized helicoidal parameters and of axis curvature for irregular nucleic acids. *J. Biomol. Struct. Dyn.*, **6**, 63–91.
53. Uljanov,N.B., Gorin,A.A., Zhurkin,V.B., Chen,B.-C., Sarma,M.H. and Sarma,R.H. (1992) Systematic study of nuclear Overhauser effects vis-a-vis local helical parameters, sugar puckers, and glycosidic torsions in B DNA: insensitivity of NOE to local transitions in B DNA oligonucleotides due to internal structural compensations. *Biochemistry*, **31**, 3918–3930.
54. Metzler,W.J., Wang,C., Kitchen.,D.B., Levy,R.M. and Pardi,A. (1990) Determining local conformational variations in DNA. Nuclear magnetic resonance structures of the DNA duplexes d(CGCCTAATCG) and d(CGTCACGCGC) generated using back-calculation of the nuclear Overhauser effect spectra, a distance geometry algorithm and constrained molecular dynamics. *J. Mol. Biol.*, **214**, 711–736.